

Can Vision-Language Models Count? A Synthetic Benchmark and Analysis of Attention-Based Interventions

Saurav Sengupta *

Nazanin Moradinasab *

Donald E. Brown

School of Data Science, University of Virginia
Charlottesville, Virginia, USA

{ss4yd, nm4wu, mru2xn, deb}@virginia.edu

Abstract

Recent research suggests that Vision Language Models (VLMs) often rely on inherent biases learned during training when responding to queries about visual properties of images. These biases are exacerbated when VLMs are asked highly specific questions that require them to focus on particular areas of the image in tasks such as counting. We build upon this research by developing a synthetic benchmark dataset and evaluation framework to systematically determine how counting performance varies as image and prompt properties change. Using open-source VLMs, we then analyze how attention allocation fluctuates with varying input parameters (e.g. number of objects in the image, objects color, background color, objects texture, background texture, and prompt specificity). We further implement attention-based interventions to modulate focus on visual tokens at different layers and evaluate their impact on counting performance across a range of visual conditions. Our experiments reveal that while VLM counting performance remains challenging, especially under high visual or linguistic complexity, certain attention interventions can lead to modest gains in counting performance.

1. Introduction

While specialized object counting methods consistently outperform Vision Language Models (VLMs) on controlled benchmarks—including SAM-based detection frameworks like PseCo that leverage foundation models for class-agnostic counting [11], multi-modal open-world counters such as CountGD that achieve state-of-the-art accuracy through grounding and visual exemplars [2], and density estimation approaches like CrowdDiff that employ diffusion models for high-fidelity crowd density prediction [17], robust counting capabilities can be essential for VLMs. Unlike task-specific counters that require category-specific

training or few-shot examples, VLMs must support compositional queries where numerosity estimation is embedded within complex reasoning chains. From both cognitive and architectural perspectives, accurate understanding of numbers of objects in an image can be a foundational capability for general visual intelligence that can help improve downstream tasks in robotics, medical imaging and more [18, 19]. This work provides a systematic quantification of current open-source VLM performance in object counting, and investigates the critical role attention plays in their success or failure.

Research on VLM counting performance from Guo *et al.* and Aghisi *et al.* [1, 8] show that VLMs are not proficient in counting. Guo *et al.* use 3 ‘levels’ of images and prompts with each succeeding ‘level’ being in increasing order of complexity. They measure accuracy and relative error when compared to the ground truth count. Aghisi *et al.* [1] evaluate the use of reasoning in improving counting performance and probe the language model for which layers contribute most to getting a more accurate count.

In parallel with these efforts, we create a set of synthetic images designed to evaluate VLM counting performance. Our work differs from existing work not by merely expanding the evaluation criteria, but by providing a fine-grained diagnostic framework. Our approach provides a comprehensive analysis across four key dimensions: (1) prompt specificity, (2) visual complexity via variations in texture and color across backgrounds and objects, (3) systematic count ranges from 0-50 in increments of 10, and (4) attention distribution over vision tokens. Crucially, this framework allows us to correlate specific visual and linguistic inputs (1-3) with their mechanistic effects on model internals (4). We evaluate three open-source VLMs that perform strongly on established VLM benchmarks: 1. **Qwen2.5-VL**[21] 2. **Kimi-VL-A3B-Instruct** [20] and 3. **InternVL3-9B** [5]. Their open-source nature enables detailed introspection into model internals. This multifaceted

*These authors contributed equally.

evaluation framework enables a more precise, mechanistic understanding of VLM counting capabilities and failure modes. We use a subset of this data to investigate how modifying attention over vision tokens changes VLM counting performance over our evaluation dataset.

In summary, in this paper we:

1. Create a synthetic counting dataset that allows us to evaluate VLMs counting performance. The images, while unchallenging for modern computer vision, reveal different failure modes of VLM counting performance. They allow us to isolate specific characteristics of the image and control for other variables to investigate which part of the input prompt and input image might have contributed to the failure mode.
2. Characterize the chosen VLM’s counting performance along a) increasing prompt specificity, b) object shapes and colors, c) background colors and textures, and d) distribution of attention over vision tokens.
3. Building upon our analysis, we investigate attention modification over visual tokens, specifically in the language decoder part of the VLM. We move beyond passive observation to evaluate if actively modifying the attention over vision tokens causally contributes to increased counting accuracy.

2. Related Work

Recent research has revealed significant limitations in Vision Language Models’ counting capabilities. Vo et al.[22] demonstrate that state-of-the-art VLMs like Open AI’s o3 [16] and Google DeepMind’s Gemini 2.5 Pro [7] exhibit strong prior knowledge biases that severely compromise counting accuracy, as models default to memorized patterns rather than analyzing visual features. This bias extends to general visual understanding. Guo et al. [8] systematically show that VLMs struggle to count beyond 20 objects, with performance deteriorating as scene complexity increases. Aghisi et al. [1] identify that reasoning chains can partially improve counting, with middle transformer layers being most critical for accurate enumeration.

Attention mechanisms play a crucial role in VLM visual processing. Kang et al. [12] reveal that VLMs often allocate excessive attention to irrelevant sections of the image and propose a method to redistribute the attention to more relevant areas. An et al. [3] demonstrate that object hallucinations can be mitigated through specialized attention mechanisms that better integrate global and local visual features. Furthermore, synthetic data has proven valuable for controlled VLM evaluation. Several studies have examined the vision understanding of VLMs by evaluating their Visual Question Answering (VQA) capabilities using synthetic imaging data [10, 14, 15] or by visualizing Attention Guided Class Activation Maps (AG-CAM) on chart-based data [6].

Our work builds upon these foundations by providing a more granular, diagnostic benchmark. We systematically isolate the impact of *visual properties* (e.g., textures, colors, shapes), allowing us to pinpoint failure modes related to visual complexity rather than just compositional logic. We also implement a set of primitive interventions (e.g., Amplify, Suppress) to better understand the mechanisms of counting failure and to evaluate their potential to improve counting accuracy.

3. Methodology

3.1. Synthetic Evaluation Dataset

We create a collection of synthetic datasets, each consisting of images and corresponding prompts, to facilitate a systematic examination of VLMs. Each dataset is designed to evaluate distinct aspects of the input data—both visual and textual. Our generation process begins with a **baseline dataset** consisting of 512×512 pixel images containing non-overlapping black circular objects on a pure white background. We generate 50 images for this initial configuration. From this baseline, we iterate by varying two primary factors: 1. **Object Numerosity:** We vary the object counts in buckets of 10, ensuring each bucket is equally represented. This allows us to evaluate how VLM performance degrades as the number of objects successively increases. 2. **Visual Properties:** We employ a controlled variable methodology. While preserving the object locations from the base dataset, we systematically vary only one feature at a time from the set: {object shape, object color, object texture, background color, background texture}. All other variables are held constant. This systematic generation framework allows us to measure and visualize variations in model performance and shifts in attention allocation. By manipulating a single dimension at a time, we can isolate the specific effects of each visual or textual property on the model’s counting capabilities.

3.2. Evaluation Criteria

We evaluate VLM counting performance using two primary metrics: Accuracy and Mean Relative Count Error (MRCE). MRCE is defined as:

$$\text{MRCE} = \frac{1}{N} \sum_{i=1}^N \frac{|c_{\text{pred}}^{(i)} - c_{\text{true}}^{(i)}|}{c_{\text{true}}^{(i)}} \quad (1)$$

where N is the number of samples, $c_{\text{pred}}^{(i)}$ is the predicted count for sample i , and $c_{\text{true}}^{(i)}$ is the ground truth count for sample i .

We assess these metrics across four primary experimental axes:

Increasing prompt specificity. We analyze model sensitivity to prompt phrasing using a “prompt ladder,” where we progressively add descriptive details (e.g., color, texture) to a generic counting prompt. This allows us to examine how incremental linguistic specificity influences model performance. Example prompts are provided in Table 9. Table 1. Example prompts used when image has different Object Texture.

ID	Example Prompt Text	Logical Role / Cognitive Cue
P1	Count the number of distinct objects in this image...	Baseline: Generic unconstrained prompt.
P2	Count the number of {color} color objects in this image...	Single (Simple) Attribute: Simple Cue (Color) - Replace {color} with object colors (“Blue-green” for default).
P3	Count the number of objects with {pattern} pattern in this image ...	Single (Complex) Attribute: Complex (Texture). Replace {pattern} with “dots”, “linear gradient”, “checkerboard”, “vertical stripe”, etc.
P4	Count the number of {pattern} pattern with {color} color objects in this image...	Compositional (Target): Binding (Complex + Simple). Tests binding a simple cue with a complex one.
P5	Count the number of {pattern} pattern with {color} color {shape} in this image...	Compositional (High Load): Multi-attribute binding under high cognitive load.

Sensitivity to Visual Properties. We evaluate performance by systematically varying a single image characteristic at a time (e.g., object color, object texture, background color, background texture) while holding all other factors constant. This allows us to isolate the impact of specific visual features on counting performance.

Object Counts Ranges. We analyze how VLM performance varies across different object count intervals (e.g., 0–9, 10–19, . . . , 40–50) to identify the threshold at which a model’s counting capabilities begin to deteriorate.

Attention over vision tokens. We quantify how much attention is given to visual tokens in each of the above sce-

narios to glean insight as to how self-attention is choosing to allocate attention over objects in the image.

3.3. Impact of attention redistribution over counting performance

VLMs exhibit systematic failures in counting tasks, with performance degrading sharply as object count increases (See Section 4.3). We hypothesize that this limitation stems from diffuse attention mechanisms that fail to distinguish and distinctly represent each object instance, leading to feature conflation and under-counting. To investigate this, we move from passive observation to active intervention. We evaluate how self-attention on vision tokens during decoding affects counting performance. We systematically modify how much attention each layer of the language model decoder pays to each token in the vision input, measuring the resulting impact on accuracy and MRCE. Since our method operates at inference time without requiring retraining, it is broadly applicable across VLM architectures.

We investigate five distinct attention reweighting strategies to manipulate how vision-language models allocate attention between visual and textual tokens during generation. Let $\mathbf{A} \in \mathbb{R}^{H \times Q \times K}$ denote the attention weight matrix for a given layer, where H is the number of attention heads, Q is the query sequence length, and K is the key sequence length. We denote the visual token positions as $V = \{v_{\text{start}}, \dots, v_{\text{end}}\}$ where visual tokens typically occupy the prefix of the sequence.

Amplify. This strategy increases attention weights to visual tokens by a multiplicative factor $\alpha > 1$:

$$\tilde{A}_{h,i,j} = \begin{cases} \alpha \cdot A_{h,i,j} & \text{if } j \in V \\ A_{h,i,j} & \text{otherwise} \end{cases} \quad (2)$$

followed by renormalization: $\tilde{A}_{h,i,:} \leftarrow \tilde{A}_{h,i,:} / \sum_k \tilde{A}_{h,i,k}$. This strategy strengthens visual grounding by encouraging stronger connections to image features. In our experiments, we use $\alpha = 2.0$.

Suppress. Conversely, this strategy reduces attention to visual tokens, forcing greater reliance on linguistic context :

$$\tilde{A}_{h,i,j} = \begin{cases} \beta \cdot A_{h,i,j} & \text{if } j \in V \\ A_{h,i,j} & \text{otherwise} \end{cases} \quad (3)$$

where $0 < \beta < 1$, followed by renormalization. We set $\beta = 0.5$ in our experiments.

Focus. This strategy creates an extreme form of visual attention by largely eliminating attention to non-visual tokens:

$$\tilde{A}_{h,i,j} = \begin{cases} A_{h,i,j} & \text{if } j \in V \\ \epsilon & \text{otherwise} \end{cases} \quad (4)$$

where $\epsilon = 10^{-10}$ is a small constant to maintain numerical stability. After renormalization, attention is effectively

concentrated solely on visual tokens, forcing direct visual conditioning at each generation step.

Balance. This strategy enforces a target distribution between visual and textual attention. Given the desired visual attention ratio r_v^{target} (we use $r_v^{\text{target}} = 0.4$) and the current ratio: $r_v^{\text{current}} = \frac{\sum_{j \in V} A_{h,i,j}}{\sum_k A_{h,i,k}}$, we apply a corrective scaling:

$$\tilde{A}_{h,i,j} = \begin{cases} \gamma \cdot A_{h,i,j} & \text{if } j \in V \\ A_{h,i,j} & \text{otherwise} \end{cases} \quad (5)$$

where $\gamma = r_v^{\text{target}} / r_v^{\text{current}}$, followed by renormalization. This preserves visual–textual attention balance and prevents over- or under-reliance on visual information.

Visual Mask Amplify. Let $\mathbf{M} \in \{0, 1\}^{H_{\text{img}} \times W_{\text{img}}}$ denote a binary object mask obtained from an off-the-shelf segmentation model (e.g., SAM [13] or Mask R-CNN [9]). For a vision transformer with patch size p , we partition the image into a grid of $N_h \times N_w$ patches where $N_h = H_{\text{img}}/p$ and $N_w = W_{\text{img}}/p$.

For each visual token v_i corresponding to patch coordinates (r, c) , we compute the **object overlap ratio**:

$$\rho_i = \frac{1}{p^2} \sum_{x=rp}^{(r+1)p-1} \sum_{y=cp}^{(c+1)p-1} \mathbf{M}(x, y) \quad (6)$$

which measures the fraction of the patch covered by object regions. We define the set of object-relevant tokens as:

$$V_{\text{obj}} = \{v_i \in V : \rho_i > \tau\} \quad (7)$$

where τ is an overlap threshold (we use $\tau = 0.1$ to capture patches with at least 10% object coverage).

The visual mask amplify strategy then applies selective amplification:

$$\tilde{A}_{h,i,j} = \begin{cases} \alpha_{\text{obj}} \cdot A_{h,i,j} & \text{if } j \in V_{\text{obj}} \\ \alpha_{\text{bg}} \cdot A_{h,i,j} & \text{if } j \in V \setminus V_{\text{obj}} \\ A_{h,i,j} & \text{otherwise} \end{cases} \quad (8)$$

followed by renormalization. We test $\alpha_{\text{obj}} = 2.0$ to strongly emphasize objects and $\alpha_{\text{bg}} = 0.5$ to suppress background, creating a high-contrast attention distribution that prioritizes semantically meaningful content. We also test an ablation of this strategy without background suppression.

Each strategy was applied selectively to different layers, enabling fine-grained control over the model’s multimodal fusion process. We denote a configuration as $\mathcal{C} = \{\sigma_1, \dots, \sigma_L\}$ where $\sigma_\ell \in \{\text{amplify, suppress, focus, balance, visual_mask_amplify}\}$ specifies the strategy for layer ℓ .

4. Results

4.1. Effects of Prompt Specificity

Through our “prompt ladder” framework—where we systematically vary specificity from generic object counting to

Table 2. Effect of prompt specificity on counting accuracy and MRCE. Prompt 1 (gray cells) serves as the baseline. For Accuracy: darker red indicates greater improvements, darker blue indicates larger drops. For MRCE: darker red indicates greater error reduction (better), darker blue indicates increased relative error (worse). “Bg” = *Background*, “Obj” = *Object*.

Cat.	Feat.	Prompts	Qwen32b		Qwen7b		InternVL		Kimi	
			Acc	MRCE	Acc	MRCE	Acc	MRCE	Acc	MRCE
Bg	color	P1	0.22	0.133	0.223	0.242	0.167	0.133	0.247	0.162
		P2	+0.047	-0.032	+0.013	-0.087	-0.010	+0.026	+0.020	-0.079
		P3	+0.033	-0.038	-0.003	-0.071	+0.013	+0.029	+0.033	-0.086
Bg	texture	P1	0.182	0.282	0.09	0.638	0.213	0.227	0.169	0.452
		P2	-0.003	-0.091	+0.078	-0.433	+0.009	-0.060	+0.095	-0.355
		P3	-0.018	-0.075	+0.078	-0.415	-0.020	+0.048	+0.076	-0.346
		P4	+0.042	-0.149	+0.062	-0.409	-0.013	+0.029	+0.069	-0.346
		P5	+0.057	-0.152	+0.057	-0.400	-0.011	+0.020	+0.067	-0.350
Obj	color	P1	0.24	0.104	0.163	0.274	0.22	0.100	0.246	0.129
		P2	-0.023	+0.021	+0.049	-0.115	-0.011	+0.030	-0.003	-0.013
		P3	-0.043	+0.002	+0.051	-0.118	-0.031	+0.034	0.000	-0.007
Obj	shape	P1	0.196	0.135	0.18	0.347	0.224	0.128	0.228	0.139
		P2	+0.004	-0.011	+0.020	-0.213	+0.020	+0.003	+0.016	+0.090
		P3	+0.024	+0.002	+0.004	-0.203	+0.024	+0.019	+0.028	-0.018
Obj	texture	P1	0.24	0.145	0.172	0.543	0.254	0.113	0.272	0.076
		P2	-0.084	+0.132	-0.006	-0.319	0.000	+0.048	-0.010	+0.067
		P3	-0.088	+0.107	-0.078	-0.266	-0.136	+0.309	-0.018	+0.027
		P4	-0.096	+0.144	-0.060	-0.238	-0.080	+0.201	-0.040	+0.090
		P5	-0.108	+0.172	-0.076	-0.219	-0.076	+0.194	-0.042	+0.098

highly detailed attribute binding—we uncover a key insight: VLM counting performance is not governed by ‘compositionality failure’ itself, but by the cognitive load of the prompt’s primary segmentation cue. This bottleneck creates an “enumerative binding failure”—a failure to count objects that the model, according to attention overlays, can perceptually ‘see’. We first establish that simple conjunction (`color+shape`) is not the primary bottleneck. As shown in Table 2, performance on this task is merely ‘unstable’ rather than catastrophic. For instance, while some models show modest gains, InternVL3-9B shows only a negligible shift in error when `shape` is specified ($\Delta \text{MRCE} = +0.003$). This indicates that while simple conjunction is a non-trivial challenge, it is not the critical failure point.

This minor instability is dwarfed by the catastrophic failure in the `object texture` task. Here, the baseline prompt (P1: “Count... objects”) is optimal (Kimi MRCE 0.076 ± 0.015). P1 succeeds because its very generality allows the model to deploy its most robust internal detector, bypassing the “cognitive sink” that *any* specific semantic cue (whether `texture`, `color`, or `shape`) creates in this task. We have direct visual evidence for this “sink” in Figure 1 when `shape` is added in P5 (`color+texture+shape`), attention overlays confirm the model’s attention to the object’s shape is absent, suppressed by the cognitive load of processing `texture` and `color`.

This paradox resolves when the prompt enables

a “Segment-then-Filter” strategy, as seen in the background texture task. Here, the P1 baseline fails (Kimi MRCE 0.452), but a simple target prompt (P2: “white objects”) makes segmentation easy and recovers all performance (Δ MRCE=−0.355). With segmentation load reduced, cognitive resources are freed for contextual filtering. Qwen32b demonstrates this capability, showing significant improvement when adding the compositional background filter (P2 → P5: Δ MRCE = −0.061; Δ Accuracy = 0.06).

These findings collectively indicate that the utility of prompt specificity is highly context-dependent. Specificity aids performance when it simplifies the primary visual segmentation task, but becomes detrimental when it introduces multi-cue processing demands that exceed the model’s cognitive capacity.

4.2. Effects of Visual Complexity

Table 3 presents the Mean Relative Count Error (MRCE) for Prompt 2—the single-attribute, color-focused prompt—across all background and object variations. The results show a clear trend: model performance degrades substantially as visual complexity increases. Models perform well under simple conditions, such as solid-colored backgrounds and plain, single-color objects, where MRCE is lowest. However, the error increases significantly when high-frequency textures (e.g., checkerboard, diagonal/vertical stripes, concentric rings) or visually heterogeneous objects (multicolor or complex patterns) are introduced. This pattern is consistent across most models, indicating that complex textures and patterns interfere with the models’ ability to reliably segment and enumerate objects. Results for Prompts 1 and 3–5 are provided in the Supplementary.

4.3. Effects of Count Magnitude

To analyze the effect of count magnitude on model accuracy, we divided all images into five discrete count bins—namely <10, 10–19, 20–29, 30–39, and 40–50 objects, as shown in Table 4. The results are collapsed across all prompt formulations, where darker blue shades indicate smaller errors. We observe a consistent trend across all models: counting performance degrades monotonically with increasing object count. In the low-count regime (<10), most models exhibit minimal error (<0.1), indicating strong reliability when few instances are present. However, as the number of objects increases, error grows non-linearly—particularly beyond 30. When separating by visual feature type, simple Color category shows the smallest deviation. In contrast, texture categories consistently exhibit the largest variance, implying that complex surface patterns interfere with spatial grouping mechanisms. Among the models, Kimi-VL-A3B-Instruct and Qwen2.5-32B-Instruct maintain the lowest relative errors

Table 3. Mean Relative Count Error (lower is better) for Prompt 2 across all patterns. “Bg” denotes *Background*, “Obj” denotes *Object* and “diag. str.” denotes diagonal stripes, “ver. str.” denotes vertical stripes, “hor. str.” denotes horizontal stripes, “con. cir.” denotes concentric circles, “lin. grad.” linear gradient, “rad. grad.” denotes radial gradient, “con. rgs.” denotes concentric rings, “cr. hatch” denotes cross hatch categories.

Cat.	Feat.	Pattern	Qwen7b	Qwen32b	Intern	Kimi
Bg	Color	blue	0.129	0.109	0.134	0.075
Bg	Color	black	0.152	0.088	0.135	0.083
Bg	Color	green	0.159	0.109	0.134	0.062
Bg	Color	gray	0.156	0.106	0.160	0.072
Bg	Color	red	0.150	0.100	0.165	0.087
Bg	Color	yellow	0.176	0.095	0.221	0.113
Bg	Texture	lin. grad.	0.138	0.105	0.077	0.078
Bg	Texture	noise	0.120	0.096	0.145	0.071
Bg	Texture	rad. grad.	0.146	0.164	0.121	0.062
Bg	Texture	cr. hatch	0.172	0.137	0.133	0.053
Bg	Texture	ver. str.	0.210	0.130	0.179	0.062
Bg	Texture	checkerboa	0.232	0.135	0.188	0.113
Bg	Texture	hor. str.	0.245	0.182	0.115	0.154
Bg	Texture	con. rgs	0.239	0.193	0.253	0.068
Bg	Texture	diag. str	0.249	0.308	0.147	0.071
Bg	Texture	bubbles	0.264	0.176	0.300	0.204
Bg	Texture	dots	0.264	0.560	0.174	0.116
Obj	Color	green	0.097	0.086	0.085	0.066
Obj	Color	red	0.126	0.115	0.088	0.063
Obj	Color	blue	0.108	0.105	0.120	0.062
Obj	Color	white	0.099	0.101	0.102	0.109
Obj	Color	yellow	0.141	0.095	0.100	0.114
Obj	Color	light gray	0.170	0.113	0.187	0.079
Obj	Color	multicolor	0.362	0.259	0.223	0.308
Obj	Shape	star	0.130	0.117	0.077	0.076
Obj	Shape	polygon	0.110	0.105	0.140	0.089
Obj	Shape	rectangle	0.089	0.128	0.198	0.079
Obj	Shape	circle	0.168	0.131	0.173	0.073
Obj	Shape	triangle	0.161	0.137	0.066	0.360
Obj	Texture	lin. grad.	0.147	0.105	0.089	0.064
Obj	Texture	con. cir.	0.134	0.104	0.116	0.074
Obj	Texture	rad. grad.	0.137	0.164	0.095	0.068
Obj	Texture	ver. str.	0.124	0.130	0.125	0.095
Obj	Texture	checkerboa	0.191	0.206	0.113	0.072
Obj	Texture	hor. str.	0.167	0.182	0.175	0.079
Obj	Texture	zigzag	0.173	0.207	0.199	0.073
Obj	Texture	diag. str.	0.270	0.308	0.150	0.060
Obj	Texture	dots	0.232	0.560	0.177	0.139
Obj	Texture	cr. hatch	0.652	0.797	0.362	0.700

overall, whereas Qwen2.5-7B-Instruct and InternVL3-9B-Instruct exhibit greater sensitivity under large-count conditions. These results demonstrate a level-dependent counting robustness: performance remains stable for small sets but declines as visual density and textural complexity increase, emphasizing the need for count-adaptive attention strategies in future architectures.

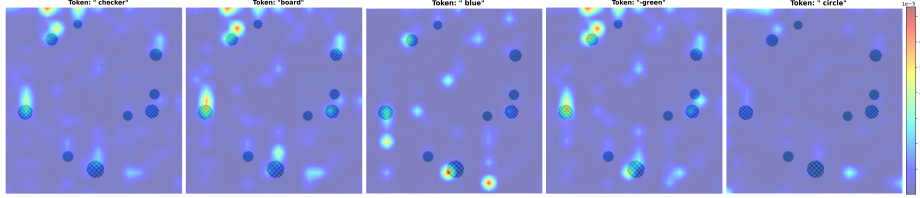


Figure 1. Token-level attention heatmaps for the compositional prompt 5 of object texture task. The high load from texture and color suppresses attention to shape

Table 4. Mean Relative Count Error (lower is better). Darker blue cells indicate smaller errors. “Bg” denotes *Background* and “Obj” denotes *Object* categories.

Cat.	Feat.	Counts	Qwen7b	Qwen32b	Intern	Kimi
Bg	Color	<10	0.039	0.050	0.099	0.020
Bg	Color	10–19	0.068	0.067	0.082	0.085
Bg	Color	20–29	0.154	0.138	0.131	0.100
Bg	Color	30–39	0.226	0.124	0.189	0.125
Bg	Color	40–50	0.451	0.170	0.253	0.201
Bg	Texture	<10	0.137	0.155	0.134	0.077
Bg	Texture	10–19	0.150	0.167	0.117	0.143
Bg	Texture	20–29	0.315	0.202	0.176	0.182
Bg	Texture	30–39	0.411	0.188	0.226	0.232
Bg	Texture	40–50	0.533	0.255	0.323	0.222
Obj	Color	<10	0.080	0.076	0.081	0.044
Obj	Color	10–19	0.097	0.103	0.078	0.090
Obj	Color	20–29	0.182	0.116	0.109	0.107
Obj	Color	30–39	0.223	0.144	0.150	0.172
Obj	Color	40–50	0.395	0.142	0.186	0.190
Obj	Shape	<10	0.087	0.079	0.044	0.032
Obj	Shape	10–19	0.094	0.112	0.079	0.097
Obj	Shape	20–29	0.156	0.185	0.168	0.135
Obj	Shape	30–39	0.282	0.151	0.164	0.174
Obj	Shape	40–50	0.395	0.132	0.223	0.220
Obj	Texture	<10	0.152	0.199	0.085	0.073
Obj	Texture	10–19	0.210	0.237	0.183	0.130
Obj	Texture	20–29	0.368	0.273	0.294	0.139
Obj	Texture	30–39	0.422	0.247	0.341	0.156
Obj	Texture	40–50	0.515	0.323	0.412	0.162

4.4. Attention over Vision Tokens

To investigate how linguistic variations influence the model’s spatial focus, we analyze the distribution of attention over vision tokens using five prompts for texture variations and three prompts for color variations applied to both the background and the object. Each prompt incrementally introduces visual descriptors such as color, shape, and texture (as an example in Table 9) ; That is, as we progress from P1 to P5, each subsequent prompt adds finer details describing either the object or the background, gradually increasing the linguistic specificity of the visual scene. As shown in Figure 2, both Qwen2.5-7B-Instruct and Kimi-VL-A3B-Instruct exhibit a consistent trend. For background Texture, moderate object-related de-

tail (P2–P3) increases Grad-CAM attention toward object regions ($IoU@50, \text{object}$) and reduces background attention ($IoU@50, \text{background}$), relative to the baseline prompt (P1). These prompts (P2–P3) introduce explicit object descriptors such as color and shape, which help the models better localize the target regions—consistent with the performance gains under moderate specificity in Section 4.1. In contrast, prompts including additional background-related information (P4–P5) generally reduce object Grad-CAM attention ($IoU@50, \text{object}$) compared to the base prompt, particularly in the Background Texture condition for both models. For Object Texture, Grad-CAM consistently shows enhanced localization across P2–P5, reflecting stronger grounding when object-specific cues are present. However, beyond P3, the inclusion of fine-grained texture descriptors does not further reduce the relative count error; instead, error tends to rise again—aligning with the “cognitive sink” effect from Section 4.1 where high-specificity prompts overload processing capacity. These results suggest that linguistic specificity aids in reducing counting error up to a moderate level, but excessive descriptive detail can counteract this benefit—highlighting a non-linear relationship between prompt richness and counting error reduction. Figure 3 shows that the number of objects in the image does not substantially influence the overall trend of visual attention. Both models exhibit consistent attention patterns for images containing fewer than 10 objects and for those with more than 30. In both settings, **Grad-CAM** and **LPV** attention distributions follow similar trajectories across prompts, though relative count error remains significantly lower in the <10 object condition compared to the >30 objects setting. This stability indicates that the models’ spatial grounding behavior, as guided by linguistic cues, is largely invariant to object density. Figure 3 illustrates this finding for the background-texture condition, which closely mirrors the trends reported earlier in Figure 2. The trends for the models—Qwen2.5-32B-Instruct and InternVL3-9B-Instruct— are presented in the supplementary material.

4.5. Impact of Attention Redistribution

We present the results of our layer wise attention reweighting experiments in Table 5. These interventions were tested on the background texture dataset, with results av-

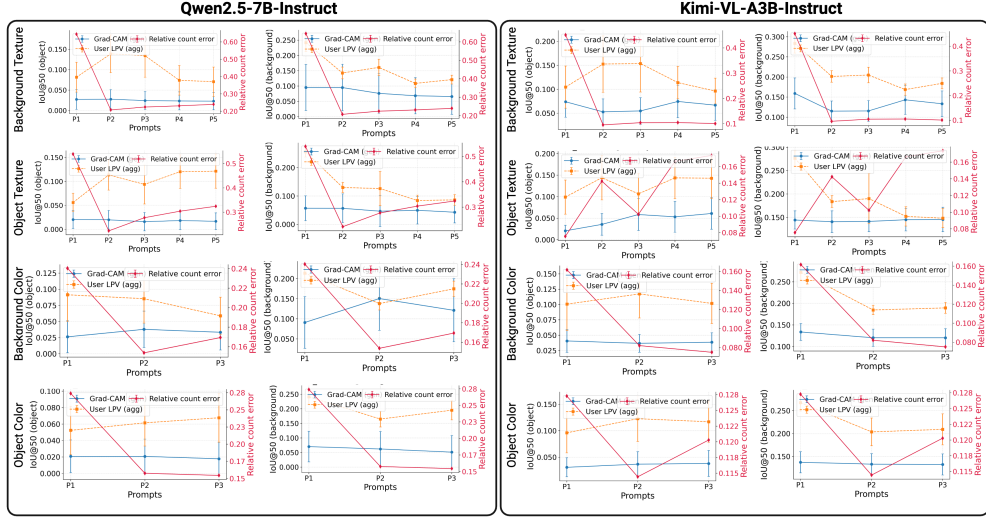


Figure 2. Visualization of the model’s attention

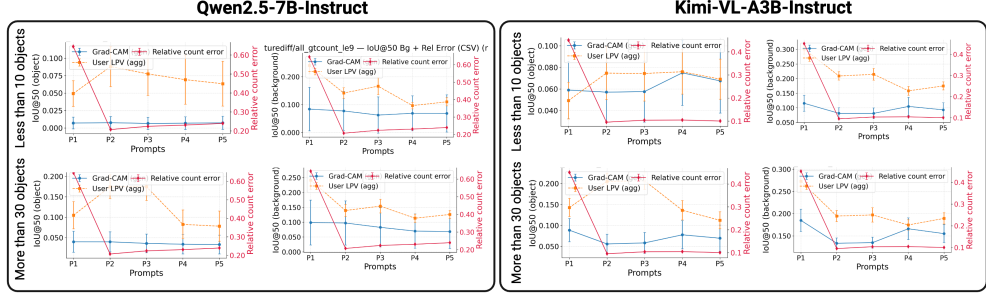


Figure 3. Visualization of the model’s attention across different background-texture patterns for images containing fewer than 10 objects or more than 30 objects.

Table 5. MRCE and accuracy results of different attention reweighting strategies. early: layers 0-7, middle: layers 8-24, late: layers 24-31 for Qwen models. early: layers 0-8, middle: layers 9-17, late: layers 18-26 for Kimi. Optimum values in bold. ‘-’ represents predictions unparsable into counts.

Strat. Class	Attention Strategy	Description	Qwen2.5 7B		Qwen3 8B		Kimi-VL-A3B	
			MRCE	Acc.	MRCE	Acc.	MRCE	Acc.
All layers modified	baseline	No modification baseline	0.7611	0.175	0.3641	0.3067	0.5193	0.218
	uniform amplify		1.2748	0.1767	0.5312	0.06	0.6056	0.182
	uniform focus	Uniformly amplify, focus, balance and suppress over vision tokens for all layers	-	-	-	-	0.8662	0.072
	uniform balance		0.817	0.18	0.4432	0.31	0.6144	0.205
	uniform suppress		0.4781	0.125	0.4107	0.0917	0.4854	0.188
Layer group modification	early visual only	Modify attn in early layer groups, keep others unchanged.	-	-	0.6072	0.0597	0.1659	0.205
	progressive visual grow	early:suppress, middle:balance, late:amplify	0.8013	0.1717	0.3221	0.3367	0.5319	0.197
	progressive visual fade	early:amplify, middle:balance, late:suppress	0.9127	0.1817	0.3736	0.3433	0.5237	0.208
	late visual retention	early,middle:balance, late:amplify	0.8172	0.1783	0.3974	0.3067	0.5874	0.202
Mask based amplify	late amplify visual mask	early, middle:unchanged, late:visual mask amplify	0.7143	0.1767	0.3563	0.3017	0.5209	0.225
	late mask bg suppress	early, middle:unchanged, late:visual mask amplify suppress bg	0.7364	0.1767	0.3309	0.3233	0.5209	0.225

eraged over all textures. We modify self-attention values either uniformly across all layers or in layer groups: `early` (layers 0-7 for Qwen, 0-8 for Kimi), `middle` (layers 8-24 for Qwen, 9-17 for Kimi), and `late` (layers 24-31 for Qwen, 18-26 for Kimi). Table 5 has descriptions for a limited number of experiments on layer wise self-attention value modification. More comprehensive experiments are present in Supplementary Material.

Our key findings are as follows:

Suppression sometimes beats amplification: Counter-intuitively, a simple uniform amplify strategy consistently degrades performance across all models. In contrast, suppressing attention over vision tokens uniformly achieves best MRCE for Qwen2.5-7B (0.48) and the second-best for Qwen3-8B (0.41). This suggests that VLMs may already over-attend to salient regions, and the problem lies in filtering out distractors rather than enhancing target features.

Architecture and Layer-Depth Dependent Strategies: Our results demonstrate that the most effective attention intervention is fundamentally linked to both the decoder’s architecture (MoE vs. Dense) and the layer depth (early vs. progressive vs. late) at which it is applied.

Kimi-VL, which uses a MoE decoder, benefits the most from early-layer adjustments. Applying attention modification before the MoE routing activates yields a substantial 68% reduction in MRCE (0.52 to 0.17), indicating that guiding the expert-selection process at its entry point is critical for accurate counting. In contrast, the dense decoders in the Qwen family respond differently. Qwen3-8B achieves its best MRCE (0.32) with progressive visual-growth strategies, whereas Qwen2.5-7B performs best under late-layer, mask-based amplification (MRCE 0.71). These results suggest that dense architectures, which propagate full information across all layers, benefit more from deeper, spatially targeted interventions during final answer generation.

Disconnect between accuracy and counting error: A striking disconnect exists between minimizing relative counting error and maximizing accuracy. For Kimi-VL, early layer visual intervention achieves the lowest MRCE (0.17) but a modest accuracy (20.5%). Conversely, a late layer mask-based methods yields a much higher MRCE (0.52) but achieves a higher accuracy of (22.5%). This dissociation suggests that accurate *enumeration* (low MRCE) may be determined by early-layer expert routing, while correct *recognition* and final answer synthesis (high accuracy) are finalized in deep layers with full visual context.

In summary, effective attention reweighting requires architecture-specific, layer-aware strategies that account for fundamental language decoder differences. MoE decoders benefit from early visual attention intervention before expert routing, while dense decoders require progressive modifications across all layers.

5. Conclusions and Future Work

This work presents a comprehensive investigation of counting capabilities in vision-language models through systematic evaluation and attention-based interventions. Our synthetic benchmark reveals that VLM counting failures stem primarily from enumerative binding failures under high cognitive load—where models can locate objects perceptually yet fail to enumerate them correctly—rather than from fundamental compositional reasoning deficits.

Three principal findings emerge. 1. Prompt specificity is non-monotonic: It only helps when it simplifies segmentation and becomes detrimental when it adds complex, multi-cue binding requirements. 2. Performance degrades with density and complexity: Counting performance predictably drops with higher object counts and complex textures. 3. Suppression can outperform amplification: Counter-intuitively, suppressing attention to visual tokens can be more effective than amplifying it, suggesting the bottleneck is filtering distractors, not enhancing targets.

Our systematic characterization of VLM counting failures and the effectiveness of layer-specific attention interventions provides both diagnostic tools and potential remediation strategies for the broader research community. The synthetic evaluation framework, architectural insights, and intervention methodologies we introduce offer concrete building blocks for advancing vision-language understanding, particularly in tasks requiring precise visual enumeration and compositional reasoning. Our findings motivate developing specialized attention mechanisms tailored to decoder architectures, and addressing the dissociation between counting accuracy and MRCE through hybrid training objectives. Interpretable probes could further identify network components responsible for enumeration versus classification, providing crucial insights for architectural improvements.

6. Limitations

While our controlled synthetic benchmarks enable precise failure mode analysis, extending this framework to real-world scenarios with occlusion, varying scales, and complex spatial arrangements remains essential. Our evaluation framework did not incorporate reasoning-augmented versions of the tested models, such as Kimi-VL-A3B-Thinking [20], which employ extended chain-of-thought (CoT) reasoning. Our evaluation exclusively examines open-source VLMs—while methodologically necessary for attention introspection—limits our assessment of the broader landscape of VLM counting capabilities. Proprietary models may also employ inference-time techniques we cannot observe or replicate. Furthermore, our attention interventions assume standard transformer architectures; if frontier models employ attention variants (e.g., mixture of depths or sparse attention patterns), our strategies may not directly transfer.

Finally, while synthetic data enables controlled variable manipulation, it may not fully capture the visual complexity of natural images, potentially limiting the generalizability of our findings.

References

- [1] Simone Alghisi, Gabriel Roccabruna, Massimo Rizzoli, Seyed Mahed Mousavi, and Giuseppe Riccardi. [de–re] constructing vlms’ reasoning in counting. *arXiv preprint arXiv:2510.19555*, 2025. [1](#) [2](#)
- [2] Niki Amini-Naieni, Tengda Han, and Andrew Zisserman. Countgd: Multi-modal open-world counting. *Advances in Neural Information Processing Systems*, 37:48810–48837, 2024. [1](#)
- [3] Wenbin An, Feng Tian, Sicong Leng, Jiahao Nie, Haonan Lin, QianYing Wang, Ping Chen, Xiaoqin Zhang, and Shijian Lu. Mitigating object hallucinations in large vision-language models with assembly of global and local attention. In *Proceedings of the Computer Vision and Pattern Recognition Conference*, pages 29915–29926, 2025. [2](#)
- [4] Hila Chefer, Shir Gur, and Lior Wolf. Generic attention-model explainability for interpreting bi-modal and encoder-decoder transformers. In *Proceedings of the IEEE/CVF International Conference on Computer Vision (ICCV)*, pages 397–406, 2021. [1](#)
- [5] Zhe Chen, Jiannan Wu, Wenhui Wang, Weijie Su, Guo Chen, Sen Xing, Muyan Zhong, Qinglong Zhang, Xizhou Zhu, Lewei Lu, et al. Internvl: Scaling up vision foundation models and aligning for generic visual-linguistic tasks. In *Proceedings of the IEEE/CVF conference on computer vision and pattern recognition*, pages 24185–24198, 2024. [1](#)
- [6] Lianghan Dong and Anamaria Crisan. Probing the visualization literacy of vision language models: the good, the bad, and the ugly. *arXiv preprint arXiv:2504.05445*, 2025. [2](#)
- [7] Google. Google deepmind: Gemini 2.5 pro, 2025. <https://deepmind.google/models/gemini/pro/>. [2](#)
- [8] Xuyang Guo, Zekai Huang, Zhenmei Shi, Zhao Song, and Jiahao Zhang. Your vision-language model can’t even count to 20: Exposing the failures of vlms in compositional counting. *arXiv preprint arXiv:2510.04401*, 2025. [1](#) [2](#)
- [9] Kaiming He, Georgia Gkioxari, Piotr Dollár, and Ross Girshick. Mask r-cnn. In *Proceedings of the IEEE international conference on computer vision*, pages 2961–2969, 2017. [4](#)
- [10] Yifan Hou, Buse Giledereli, Yilei Tu, and Mrinmaya Sachan. Do vision-language models really understand visual language? *arXiv preprint arXiv:2410.00193*, 2024. [2](#)
- [11] Zhizhong Huang, Mingliang Dai, Yi Zhang, Junping Zhang, and Hongming Shan. Point segment and count: A generalized framework for object counting. In *Proceedings of the IEEE/CVF Conference on Computer Vision and Pattern Recognition*, pages 17067–17076, 2024. [1](#)
- [12] Seil Kang, Jinyeong Kim, Junhyeok Kim, and Seong Jae Hwang. See what you are told: Visual attention sink in large multimodal models. *arXiv preprint arXiv:2503.03321*, 2025. [2](#)
- [13] Alexander Kirillov, Eric Mintun, Nikhila Ravi, Hanzi Mao, Chloe Rolland, Laura Gustafson, Tete Xiao, Spencer Whitehead, Alexander C Berg, Wan-Yen Lo, et al. Segment anything. In *Proceedings of the IEEE/CVF international conference on computer vision*, pages 4015–4026, 2023. [4](#)
- [14] Kang-il Lee, Minbeom Kim, Seunghyun Yoon, Minsung Kim, Dongryeol Lee, Hyukhun Koh, and Kyomin Jung. Vlind-bench: Measuring language priors in large vision-language models. *arXiv preprint arXiv:2406.08702*, 2024. [2](#)
- [15] Tony Lee, Haoqin Tu, Chi H Wong, Wenhao Zheng, Yiyang Zhou, Yifan Mai, Josselin S Roberts, Michihiro Yasunaga, Huaxiu Yao, Cihang Xie, et al. Vhelm: A holistic evaluation of vision language models. *Advances in Neural Information Processing Systems*, 37:140632–140666, 2024. [2](#)
- [16] OpenAI. Open ai: Introducing openai o3 and o4-mini, 2025. <https://openai.com/index/introducing-o3-and-o4-mini/>. [2](#)
- [17] Yasiru Ranasinghe, Nithin Gopalakrishnan Nair, Wele Gedara Chaminda Bandara, and Vishal M Patel. Crowd-diff: Multi-hypothesis crowd density estimation using diffusion models. In *Proceedings of the IEEE/CVF Conference on Computer Vision and Pattern Recognition*, pages 12809–12819, 2024. [1](#)
- [18] Ji Seung Ryu, Hyunyoung Kang, Yuseong Chu, and Sejung Yang. Vision-language foundation models for medical imaging: a review of current practices and innovations. *Biomedical Engineering Letters*, pages 1–22, 2025. [1](#)
- [19] Rui Shao, Wei Li, Lingsen Zhang, Renshan Zhang, Zhiyang Liu, Ran Chen, and Liqiang Nie. Large vlm-based vision-language-action models for robotic manipulation: A survey. *arXiv preprint arXiv:2508.13073*, 2025. [1](#)
- [20] Kimi Team, Angang Du, Bohong Yin, Bowei Xing, Bowen Qu, Bowen Wang, Cheng Chen, Chenlin Zhang, Chenzhuang Du, Chu Wei, Congcong Wang, Dehao Zhang, Dikang Du, Dongliang Wang, Enming Yuan, Enzhe Lu, Fang Li, Flood Sung, Guangda Wei, Guokun Lai, Han Zhu, Hao Ding, Hao Hu, Hao Yang, Hao Zhang, Haoning Wu, Haotian Yao, Haoyu Lu, Heng Wang, Hongcheng Gao, Huabin Zheng, Jiaming Li, Jianlin Su, Jianzhou Wang, Jiaqi Deng, Jiezhang Qiu, Jin Xie, Jinhong Wang, Jingyuan Liu, Junjie Yan, Kun Ouyang, Liang Chen, Lin Sui, Longhui Yu, Mengfan Dong, Mengnan Dong, Nuo Xu, Pengyu Cheng, Qizheng Gu, Runjie Zhou, Shaowei Liu, Sihan Cao, Tao Yu, Tianhui Song, Tongtong Bai, Wei Song, Weiran He, Weixiao Huang, Weixin Xu, Xiaokun Yuan, Xingcheng Yao, Xingzhe Wu, Xinxing Zu, Xinyu Zhou, Xinyuan Wang, Y. Charles, Yan Zhong, Yang Li, Yangyang Hu, Yanru Chen, Yejie Wang, Yibo Liu, Yibo Miao, Yidao Qin, Yimin Chen, Yiping Bao, Yiqin Wang, Yongsheng Kang, Yuanxin Liu, Yulun Du, Yuxin Wu, Yuzhi Wang, Yuzi Yan, Zaida Zhou, Zhaowei Li, Zhejun Jiang, Zheng Zhang, Zhilin Yang, Zhiqi Huang, Zihao Huang, Zijia Zhao, and Ziwei Chen. Kimi-VL technical report, 2025. [1](#) [8](#)
- [21] Qwen Team. Qwen2.5-vl, 2025. [1](#)
- [22] An Vo, Khai-Nguyen Nguyen, Mohammad Reza Taesiri, Vy Tuong Dang, Anh Totti Nguyen, and Daeyoung Kim. Vision language models are biased, 2025. [2](#)

Can Vision-Language Models Count? A Synthetic Benchmark and Analysis of Attention-Based Interventions

Supplementary Material

7. Layer-wise Propagation of Visual attention

Gradient-weighted attention. Inspired by Chefer et al. [4] propose, we propose a lightweight gradient-weighted relevance propagation(LPV) for autoregressive VLMs that turns layer-wise attentions into token-level relevance maps by using gradient weighting and cross-layer diffusion. For each Transformer layer ℓ , let $A^{(\ell)} \in \mathbb{R}^{H \times S \times S}$ be the multi-head attention (post-softmax) and let

$$G^{(\ell)} = \frac{\partial \mathcal{L}}{\partial A^{(\ell)}}$$

be its gradient obtained from a token-level cross-entropy loss on selected output positions. Noisy negative signals in the gradient are suppressed using a ReLU:

$$\tilde{G}^{(\ell)} = \text{ReLU}(G^{(\ell)}).$$

We then form a gradient-weighted attention map by element-wise interaction and heads averaging:

$$H^{(\ell)} = \frac{1}{H} \sum_{h=1}^H (A_h^{(\ell)} \odot \tilde{G}_h^{(\ell)}).$$

To preserve self-information paths, we add the identity and apply row-normalize to obtain a row-stochastic per-layer relevance transition:

$$M^{(\ell)}(i, j) = \frac{H^{(\ell)}(i, j) + \delta_{ij}}{\sum_k (H^{(\ell)}(i, k) + \delta_{ik})}.$$

Cross-layer joint relevance. We compose the last K layers to aggregate both deep semantics and shallow localization:

$$C = \prod_{\ell=L-K+1}^L M^{(\ell)}.$$

For any given output token at index t , the corresponding row $C[t, :]$ gives a fine-grained relevance distribution over all input tokens (textual and visual) that contribute to the prediction of that specific token.

Differences from Chefer et al. [4]. Our formulation follows the gradient-weighted attention idea and cross-layer composition of Chefer et al., but is tailored to autoregressive VLMs: (1) **Token-specific supervision.** We supervise a token-level cross-entropy on a *selected* set of decoding steps

and collect $\{\nabla A^{(\ell)}\}$ in a single backward pass, enabling token/time-step-specific attribution and natural multi-token aggregation. (2) **Per-layer row-stochastic transitions.** We explicitly enforce row-stochastic $M^{(\ell)}$ by adding the identity and applying row normalization at each layer, which stabilizes deep products and improves robustness. (3) **Controllable depth.** We optionally compose only the last K layers to trade interpretability depth for stability and speed without modifying model internals.

Why not plain attention rollout? Our method provides more faithful and selective relevance maps compared to simpler methods like Attention Rollout. Plain Attention rollout composes raw attentions and is class-/token-agnostic. It highlights tokens the model “looked at” (high A), but not necessarily tokens that *influenced* the specific prediction. Our gradient-weighted diffusion emphasizes attention edges that are both *used* (large A) and *useful for the current prediction* (large positive ∇A), yielding more selective and faithful relevance maps that adapt naturally to multi-token, multi-modal settings.

8. Attention Reweighting in Qwen Models

8.1. Attention Reweighting in Grouped Query Attention Architecture

Qwen 2.5 and Qwen 3 models employ Grouped Query Attention (GQA), which differs from standard Multi-Head Attention by using fewer key-value heads than query heads to reduce computational cost. Specifically, with $H = 32$ attention heads and $K = 8$ key-value heads, each KV head is shared across $G = H/K = 4$ query heads. This architecture necessitates special handling during attention reweighting. After projecting inputs through W_q , W_k , and W_v , the resulting tensors have shapes $\mathbf{Q} \in \mathbb{R}^{B \times L \times Hd}$ and $\mathbf{K}, \mathbf{V} \in \mathbb{R}^{B \times L \times Kd}$, where B is batch size, L is sequence length, and d is head dimension. Before computing attention, we reshape these to $\mathbf{Q} \in \mathbb{R}^{B \times H \times L \times d}$ and $\mathbf{K}, \mathbf{V} \in \mathbb{R}^{B \times K \times L \times d}$. The key-value heads must then be repeated via `repeat_kv(V, G)` to obtain $\mathbf{V}' \in \mathbb{R}^{B \times H \times L \times d}$ by expanding along a new dimension and reshaping: $\mathbf{V}' = \text{reshape}(\mathbf{V}[:, :, \text{None}, :, :].expand(B, K, G, L, d), [B, H, L, d])$. This ensures dimensional compatibility when applying reweighted attention weights $\tilde{\mathbf{A}} \in \mathbb{R}^{B \times H \times L \times L}$ to compute the output $\mathbf{O} = \tilde{\mathbf{A}} \mathbf{V}'$. Our implementation maintains a full cache of value projections across generation steps, repeats the KV heads

appropriately, applies the reweighting strategy to the attention weights, recomputes the attention output with modified weights, and finally applies the output projection W_o . This approach preserves the efficiency benefits of GQA while enabling fine-grained control over visual-textual attention distribution across all H query heads.

8.2. Attention Reweighting Experiments

We experiment with more comprehensive layer based configurations to measure the impact of changing attention values over different layers. In all experiments we use the same prompt: "Count the number of objects in this image. Answer the count within curly brackets, eg. {10}".

8.2.1. Experimental Configurations

Layer Groups.

- **Early (0–7):** Feature extraction—low-level visual patterns and syntactic structure
- **Middle (8–23):** Semantic integration—multimodal fusion and object relationships
- **Late (24–31):** High-level reasoning—global reasoning and linguistic refinement

We evaluate 19 attention reweighting configurations across six categories:

Baseline.

- `baseline`: No modification—standard model inference

Uniform Strategies (all layers).

- `uniform_amplify`: 2 \times visual attention throughout
- `uniform_suppress`: 0.5 \times visual attention throughout
- `uniform_focus`: Exclusive visual attention throughout
- `uniform_balance`: Maintained 40% visual ratio throughout

Progressive Strategies (layer-wise transitions).

- `progressive_visual_fade`: Strong \rightarrow balanced \rightarrow weak visual (amplify/balance/suppress)
- `progressive_visual_grow`: Weak \rightarrow balanced \rightarrow strong visual (suppress/balance/amplify)

Localized Strategies (group-specific).

- `early_visual_only`: Focus early layers, suppress middle-late
- `middle_visual_boost`: Amplify middle layers, balance elsewhere
- `late_visual_retention`: Amplify late layers, balance elsewhere
- `extreme_visual_early`: Focus first 37.5% of layers (0–11), balance rest

- `extreme_text_late`: Suppress final 37.5% of layers (20–31), balance rest

Alternating Strategy.

- `alternating_amp_sup`: Layer-by-layer amplify/suppress alternation

Object-Aware Strategies (segmentation-guided).

- `early/middle/late_amplify_visual_mask`: Object amplification (2 \times) with no background suppression in respective layer groups
- `early/middle/late_amplify_visual_mask_bg_suppress`: Object amplification (2 \times) with strong background suppression (0.5 \times) in respective layer groups

Findings: Tab. 6 presents Qwen3-VL-8B-Instruct MRCE and accuracy results for the background texture dataset across different object count buckets. We do not include the bubbles (Fig. 7k) texture since it confuses all VLMs into counting the bubbles as objects leading to high errors.

Progressive growth strategies (`progressive_visual_grow`, mean MRCE 0.37) and late-stage object masked amplification with background suppression (`late_amplify_visual_mask_bg_suppress`, mean MRCE 0.35) consistently outperform the baseline (0.33 MRCE), showing that gradual, layer-wise amplification of visual tokens while suppressing background information improves counting accuracy. The performance degradation across count buckets—from near-perfect accuracy in the 0–10 range (MRCE \sim 0.02, Acc \sim 0.87–0.90) to substantial errors in the 40–50 range (MRCE \sim 0.06–0.16, Acc \sim 0.08)—confirms that higher counts remain challenging even with attention reweighting, though our best methods maintain more graceful degradation than baseline. Critically, our experiments with aggressive early-layer interventions (`early_visual_only`, `extreme_visual_early`) demonstrate the importance of preserving text-visual alignment, as these methods catastrophically fail (mean MRCE 0.04–0.02) by over-suppressing linguistic representations.

Tab. 7 shows results from Qwen2.5-VL-7B-Instruct. The results on the background texture dataset reveal substantially different dynamics compared to Qwen 3-VL-8B, with most attention reweighting strategies achieving marginal improvements over baseline (mean MRCE 0.14 across top performers). Object mask-guided interventions including `early_amplify_visual_mask`, `late_amplify_visual_mask_bg_suppress`, and `alternating_amp_sup` all converge to 0.14 mean MRCE with 0.19–0.20 accuracy, suggesting that Qwen 2.5's architecture may already incorporate more effective

Table 6. Qwen 3-VL-8B-Instruct MRCE and Accuracy results for different object count buckets averaged over the background texture dataset. Results sorted by Mean MRCE over all buckets. We see that object mask guided attention reweighting methods beat baseline.

Attn. Strat.	0-10		10-20		20-30		30-40		40-50		Mean	
	MRCE	Acc.	MRCE	Acc.	MRCE	Acc.	MRCE	Acc.	MRCE	Acc.	MRCE	Acc.
late_amplify_visual_mask_bg_suppress	0.02	0.87	0.05	0.5	0.09	0.17	0.09	0.11	0.12	0.11	0.07	0.35
late_amplify_visual_mask	0.02	0.87	0.05	0.44	0.1	0.13	0.09	0.15	0.14	0.06	0.08	0.33
baseline	0.02	0.87	0.05	0.42	0.09	0.2	0.1	0.12	0.14	0.06	0.08	0.33
early_amplify_visual_mask	0.02	0.89	0.05	0.47	0.09	0.2	0.1	0.13	0.14	0.06	0.08	0.35
early_amplify_visual_mask_bg_suppress	0.01	0.91	0.05	0.45	0.08	0.25	0.1	0.1	0.15	0.08	0.08	0.36
extreme_text_late	0.02	0.85	0.05	0.43	0.1	0.18	0.08	0.17	0.15	0.08	0.08	0.34
uniform_balance	0.02	0.88	0.05	0.43	0.09	0.14	0.1	0.14	0.15	0.11	0.08	0.34
progressive_visual_fade	0.02	0.85	0.04	0.48	0.08	0.25	0.09	0.13	0.18	0.16	0.08	0.37
progressive_visual_grow	0.02	0.9	0.04	0.49	0.09	0.22	0.1	0.16	0.17	0.06	0.08	0.37
late_visual_retention	0.02	0.86	0.05	0.41	0.08	0.19	0.11	0.12	0.18	0.09	0.09	0.33
alternating_amp_sup	0.03	0.77	0.07	0.28	0.1	0.16	0.09	0.15	0.17	0.07	0.09	0.29
uniform_suppress	0.1	0.42	0.17	0	0.2	0	0.17	0.02	0.14	0.06	0.16	0.1
middle_visual_boost	0.13	0.27	0.18	0.05	0.2	0.04	0.28	0.01	0.35	0.05	0.23	0.08
uniform_amplify	0.14	0.25	0.2	0.05	0.22	0.01	0.29	0	0.38	0.03	0.25	0.07
middle_amplify_visual_mask	0.1	0.39	0.17	0.09	0.22	0.06	0.32	0.01	0.54	0.01	0.27	0.11
middle_amplify_visual_mask_bg_suppress	0.1	0.38	0.17	0.1	0.26	0.01	0.36	0.01	0.6	0.01	0.3	0.1
early_visual_only	0.7	0	0.26	0.19	0.62	0	0.72	0	0.78	0	0.61	0.04
extreme_visual_early	NaN	0	NaN	0.08	NaN	0	NaN	0	NaN	0	NaN	0.02
uniform_focus	NaN	0	NaN	0	NaN	0	NaN	0	NaN	0	NaN	0

Table 7. Qwen 2.5 VL-7B-Instruct MRCE and Accuracy results for different object count buckets averaged over the background texture dataset. Results sorted by Mean MRCE over all buckets. We see that object mask guided attention reweighting methods and methods like alternating_amp_sup beat baseline in MRCE. As object counts increase, attention reweighting methods lead to modest gains from baseline performance.

Attn. Strat.	0-10		10-20		20-30		30-40		40-50		Mean	
	MRCE	Acc.	MRCE	Acc.	MRCE	Acc.	MRCE	Acc.	MRCE	Acc.	MRCE	Acc.
early_amplify_visual_mask	0.08	0.61	0.13	0.12	0.11	0.12	0.15	0.12	0.21	0.03	0.14	0.2
early_amplify_visual_mask_bg_suppress	0.09	0.57	0.13	0.11	0.1	0.15	0.15	0.12	0.22	0.01	0.14	0.19
late_amplify_visual_mask_bg_suppress	0.08	0.61	0.12	0.15	0.1	0.12	0.17	0.08	0.22	0.01	0.14	0.19
alternating_amp_sup	0.09	0.57	0.12	0.15	0.1	0.13	0.17	0.08	0.22	0.02	0.14	0.19
progressive_visual_grow	0.09	0.59	0.12	0.08	0.1	0.15	0.16	0.11	0.23	0.01	0.14	0.19
late_amplify_visual_mask	0.08	0.61	0.12	0.15	0.1	0.12	0.17	0.09	0.22	0	0.14	0.19
middle_amplify_visual_mask	0.09	0.59	0.14	0.11	0.11	0.09	0.15	0.11	0.2	0.05	0.14	0.19
baseline	0.08	0.61	0.12	0.14	0.1	0.12	0.17	0.09	0.22	0	0.14	0.19
middle_amplify_visual_mask_bg_suppress	0.09	0.57	0.14	0.05	0.11	0.13	0.16	0.09	0.2	0.05	0.14	0.18
progressive_visual_fade	0.13	0.58	0.15	0.1	0.11	0.1	0.14	0.15	0.19	0.06	0.14	0.2
uniform_balance	0.12	0.57	0.13	0.14	0.1	0.15	0.16	0.09	0.21	0.04	0.14	0.2
late_visual_retention	0.12	0.57	0.13	0.14	0.1	0.14	0.16	0.09	0.21	0.04	0.14	0.19
extreme_text_late	0.13	0.54	0.13	0.16	0.1	0.14	0.16	0.08	0.22	0.02	0.15	0.19
middle_visual_boost	0.11	0.53	0.21	0.05	0.15	0.06	0.12	0.2	0.16	0.11	0.15	0.19
uniform_amplify	0.12	0.52	0.23	0.07	0.19	0.05	0.11	0.22	0.15	0.1	0.16	0.19
uniform_suppress	0.1	0.54	0.17	0.02	0.14	0.09	0.22	0.03	0.27	0.01	0.18	0.14
early_visual_only	NaN	0	NaN	0	NaN	0	NaN	0	NaN	0	NaN	0
extreme_visual_early	NaN	0	NaN	0	NaN	0	NaN	0	NaN	0	NaN	0
uniform_focus	NaN	0	NaN	0	NaN	0	NaN	0	NaN	0	NaN	0

visual attention mechanisms that limit the potential gains from our reweighting interventions. The compressed performance distribution—with nearly all viable strategies clustering tightly around baseline—indicates that this model family exhibits greater robustness to attention modifications, though it still demonstrates the characteristic degradation pattern across count buckets (0-10 range: MRCE ~0.08-0.13, Acc ~0.57-0.61; 40-50 range:

MRCE ~0.19-0.23, Acc ~0.0-0.06). Notably, the same catastrophic failure modes persist for aggressive early-layer suppression strategies (early_visual_only, extreme_visual_early, uniform_focus), reinforcing our earlier finding that preserving text-visual alignment throughout the model is critical. These results suggest that while attention reweighting remains a viable intervention strategy, its effectiveness is highly

Table 8. KimiVL-A3B-Instruct MRCE and Accuracy results for different object count buckets averaged over the background texture dataset. Results sorted by Mean MRCE over all buckets. We see that attention reweighting methods like `uniform_suppress` and `alternating_amp_sup` beat `baseline` in both MRCE, but do not match accuracy.

Attn. Strat.	0-10		10-20		20-30		30-40		40-50		Mean	
	MRCE	Acc.	MRCE	Acc.	MRCE	Acc.	MRCE	Acc.	MRCE	Acc.	MRCE	Acc.
<code>alternating_amp_sup</code>	0.05	0.58	0.10	0.14	0.09	0.15	0.07	0.10	0.14	0.10	0.09	0.24
<code>uniform_suppress</code>	0.07	0.46	0.10	0.14	0.06	0.20	0.11	0.00	0.10	0.10	0.09	0.20
<code>early_visual_only</code>	0.07	0.54	0.10	0.07	0.09	0.10	0.15	0.10	0.11	0.10	0.10	0.21
<code>baseline</code>	0.04	0.73	0.07	0.43	0.09	0.15	0.27	0.10	0.25	0.10	0.14	0.32
<code>early_amplify_visual_mask</code>	0.05	0.69	0.07	0.43	0.12	0.10	0.32	0.05	0.20	0.10	0.15	0.29
<code>early_amplify_visual_mask_bg_suppress</code>	0.05	0.69	0.07	0.43	0.12	0.10	0.32	0.05	0.20	0.10	0.15	0.29
<code>late_amplify_visual_mask</code>	0.04	0.73	0.08	0.36	0.09	0.15	0.32	0.05	0.30	0.10	0.16	0.30
<code>late_amplify_visual_mask_bg_suppress</code>	0.04	0.73	0.08	0.36	0.09	0.15	0.32	0.05	0.30	0.10	0.16	0.30
<code>progressive_visual_grow</code>	0.04	0.73	0.14	0.21	0.12	0.10	0.23	0.00	0.30	0.10	0.16	0.26
<code>extreme_text_late</code>	0.05	0.69	0.14	0.21	0.17	0.10	0.34	0.00	0.40	0.05	0.21	0.24
<code>middle_amplify_visual_mask</code>	0.05	0.65	0.16	0.36	0.20	0.05	0.39	0.00	0.35	0.05	0.22	0.24
<code>middle_amplify_visual_mask_bg_suppress</code>	0.05	0.65	0.16	0.36	0.20	0.05	0.39	0.00	0.35	0.05	0.22	0.24
<code>late_visual_retention</code>	0.06	0.65	0.13	0.21	0.24	0.00	0.44	0.00	0.56	0.00	0.28	0.20
<code>uniform_balance</code>	0.06	0.65	0.13	0.29	0.25	0.00	0.44	0.00	0.72	0.00	0.32	0.21
<code>progressive_visual_fade</code>	0.06	0.62	0.17	0.29	0.29	0.00	0.44	0.00	0.66	0.00	0.32	0.20
<code>uniform_amplify</code>	0.06	0.62	0.23	0.00	0.29	0.00	0.46	0.00	0.78	0.00	0.35	0.16
<code>middle_visual_boost</code>	0.07	0.58	0.20	0.14	0.34	0.00	0.60	0.00	0.96	0.00	0.42	0.17
<code>extreme_visual_early</code>	0.17	0.15	0.36	0.00	0.80	0.00	1.16	0.00	1.03	0.00	0.69	0.04
<code>uniform_focus</code>	0.29	0.08	0.64	0.00	1.24	0.00	1.10	0.00	1.13	0.00	0.86	0.02

architecture-dependent, with newer model families potentially incorporating design elements that already optimize attention patterns for visual reasoning tasks, thereby reducing the headroom for external manipulation.

Tab. 8 shows result from Kimi-VL-A3B. The results on the background texture dataset reveal a striking divergence from the Qwen model families, with attention reweighting strategies exhibiting counterintuitive behavior where improvements in MRCE metrics fail to translate to accuracy gains and often cause catastrophic performance collapse. While `uniform_suppress` and `alternating_amp_sup` achieve the lowest mean MRCE (0.09) and nominally outperform `baseline` (0.14 MRCE), they paradoxically underperform in accuracy (0.20-0.24 vs. 0.32 baseline), suggesting these interventions induce a counting bias that reduces error magnitude but compromises exact match performance. More concerning, many ostensibly moderate strategies—including previously successful approaches like `progressive_visual_grow`, `late_amplify_visual_mask`, and various middle-layer interventions—cause complete accuracy collapse to 0.00 in higher count buckets (30-40 and 40-50 ranges), despite maintaining reasonable MRCE values. This pattern indicates that KimiVL’s architecture is fundamentally more brittle to attention manipulation, with interventions that successfully enhance visual attention in other models disrupting critical computational pathways in this smaller (3B parameter) architecture. The extreme sensitivity extends to aggressive strategies, where `uniform_focus` and `extreme_visual_early` produce catastrophic failures (0.86 and 0.69 mean MRCE respectively), reinforcing that

smaller VLMs may lack the representational capacity to tolerate significant attention reweighting without losing essential cross-modal reasoning capabilities that enable accurate counting.

9. Sample Images

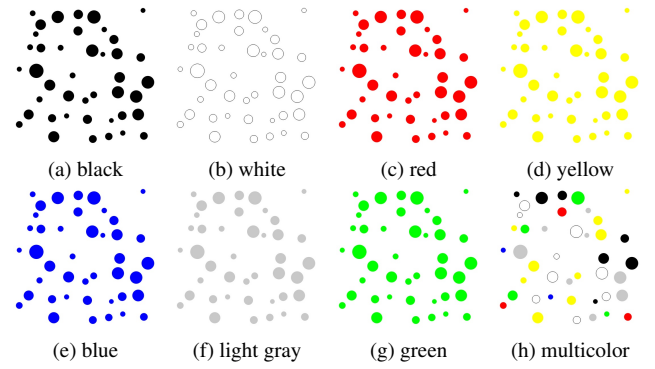


Figure 4. Example images for the **Object** category, **Color** pattern, showing different object colors.

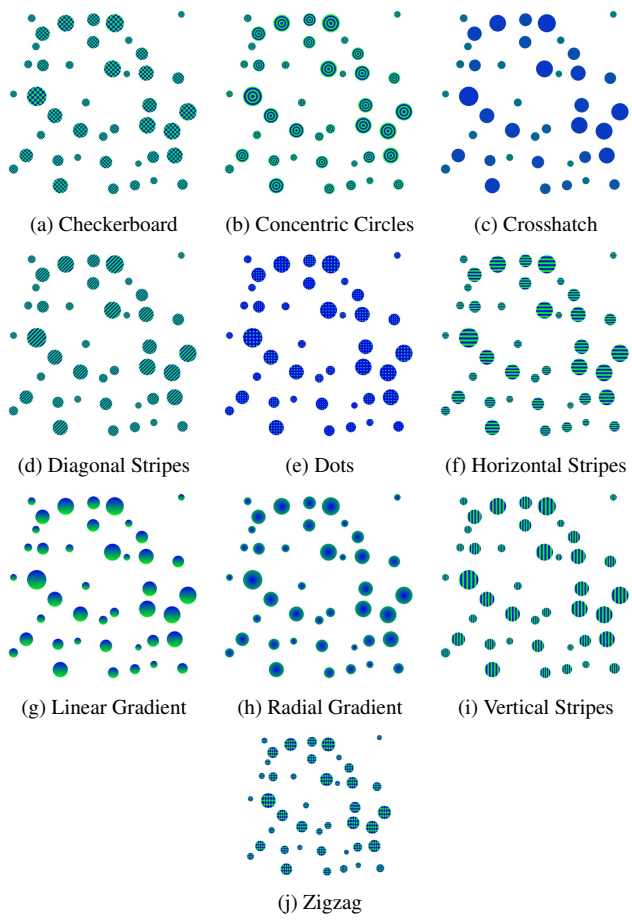


Figure 5. Example images for the **Object** category, **Texture** pattern, showing various texture types.

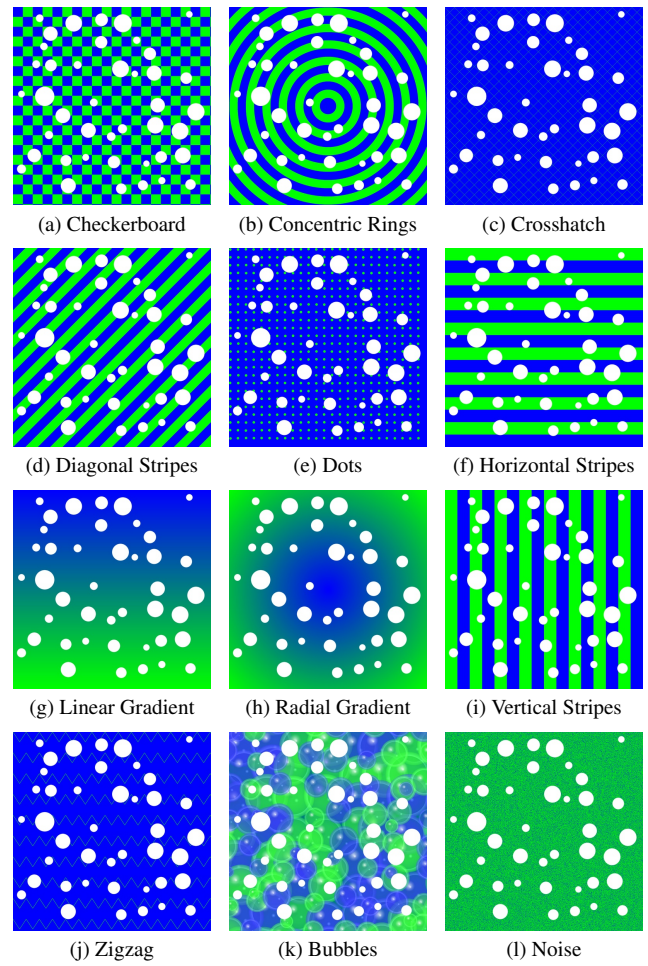


Figure 7. Example images for the **Background** category, **Texture** pattern, showing various background texture types.

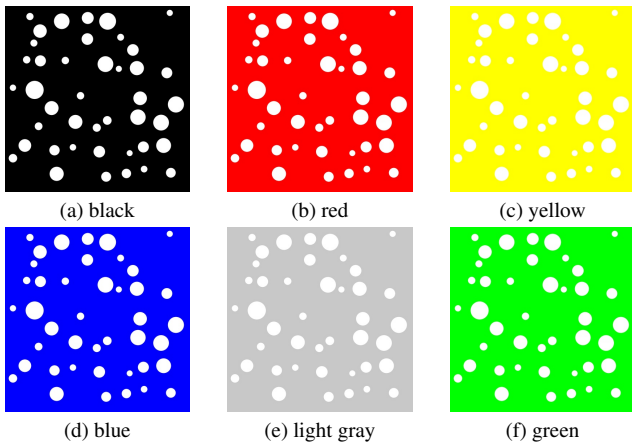


Figure 6. Example images for the **Background** category, **Color** pattern, showing different background colors.

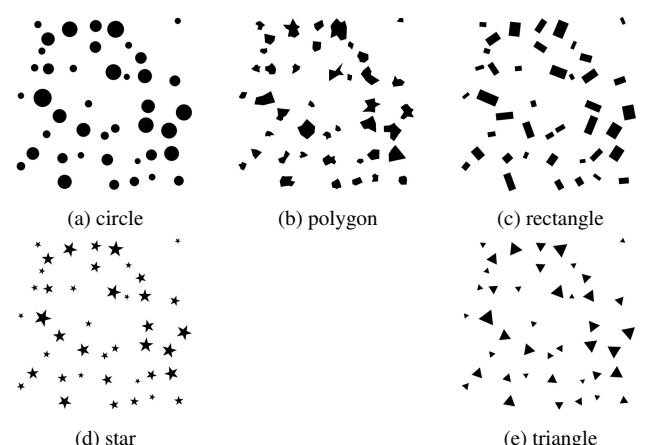


Figure 8. Example images for the **Object** category, **Shape** pattern, showing different object shapes.

10. Prompts

Table 9. Prompts used when image has different Object Color or Shape.

ID	Example Prompt Text	Logical Role / Cognitive Cue
P1	Count the number of distinct objects in this image...	Baseline: Generic unconstrained prompt.
P2	Count the number of {color} color objects in this image...	Single (Simple) Attribute: Simple target Cue (Color) - Replace {color} with object colors (blue, green, yellow, gray, multicolor, e.g.).
P3	Count the number of {color} color {shape} in this image...	Compositional (Simple) Attribute: Bind target cues (color and shape). Replace {shape} with “circles”(as default in color experiment), “squares”, “triangles”, “stars”, etc. for shape experiment. Replace {color} with “black”(as default in shape experiment), “yellow”, “red”, “blue”, etc. for color experiment.

11. Effects of Visual Complexity

Tables 12, Table 13, Table 14, and Table 15 present the Mean Relative Count Error (MRCE) for prompts 1, 3, 4, and 5, respectively.

12. Attention on Visual Tokens

Figures 9-10 shows the distribution of attention over vision as well as counting error across prompts for the Qwen2.5-32B-Instruct and InternVL3-9B. Across models (i.e. Qwen2.5-32B-Instruct, InternVL3-9B, Qwen2.5-7B, and Kimi-VL-A3B), we observe a consistent divide in how architectural scale influences the effect of prompt specificity. The smaller models—Qwen2.5-7B and Kimi-VL-A3B (3B active parameters)—in most cases show an initial reduction in relative count error as the prompts become more explicit, but this improvement saturates and eventually plateaus or even reverses. In contrast, the larger or more vision-specialized models—Qwen2.5-32B-Instruct and InternVL3-9B—do not exhibit this behavior. For these

Table 10. Prompts used when image has different Background Texture.

ID	Example Prompt Text	Logical Role / Cognitive Cue
P1	Count the number of distinct objects in this image...	Baseline: Generic unconstrained prompt.
P2	Count the number of {color} color objects in this image...	Single (Simple) Attribute: Simple Object Cue (Color) - Replace {color} with object colors (“white” for default).
P3	Count the number of {color} color {shape} in this image...	Compositional (Target): Binding (Simple+ Simple). Tests binding between two independent object attributes - Replace {shape} with object shape (“circles” for default).
P4	Count the number of {color} color objects in this image with {pattern} background...	Compositional (Target+): Binding (Complex + Simple). Tests binding a simple cue with a complex one. Tests whether the model can integrate object-level and background-level features.
P5	Count the number of {color} color shape in this image with {color}{pattern} background...	Compositional (High Load): Multi-attribute binding under high cognitive load. object color + background color (“blue-green” for default) + background pattern

models, in most cases, increasing linguistic specificity does not reliably improve performance; their error remains relatively stable or fluctuates despite more detailed instructions. These findings suggest that, unlike smaller models that benefit from increased prompt granularity, higher-capacity or vision-specialized architectures may not gain additional advantage from more explicit linguistic guidance for this counting task.

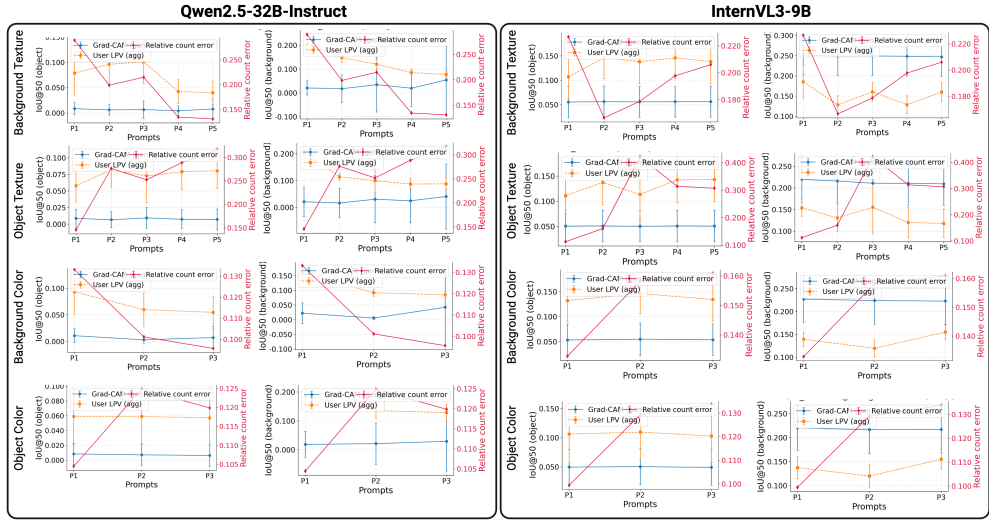


Figure 9. Visualization of the model’s attention for models the Qwen2.5-32B-Instruct and InternVL3-9B

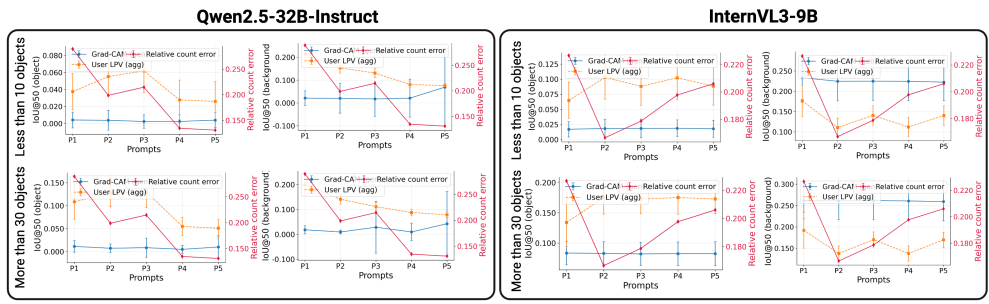


Figure 10. Visualization of the model’s attention across different background-texture patterns for images containing fewer than 10 objects or more than 30 objects for models the Qwen2.5-32B-Instruct and InternVL3-9B.

Table 11. Prompts used when image has different Background Color.

ID	Example Prompt Text	Logical Role / Cognitive Cue
P1	Count the number of distinct objects in this image...	Baseline: Generic unconstrained prompt.
P2	Count the number of {color} objects in this image with {color} background...	Compositional (Simple) Attribute: Bind target cues and contextual cue: Tests selective filtering based on a single attribute (background color), with object color("white" for default).
P3	Count the number of {color} {shape} in this image with {color} background...	Compositional (Complex) Attribute: Bind target and contextual cue: a single background attribute (background color), with two object attributes("white circle" for default).

Table 12. Mean Relative Count Error (lower is better) for Prompt 1 across all patterns. "Bg" denotes *Background*, "Obj" denotes *Object* and "diag. str." denotes diagonal stripes, "ver. str." denotes vertical stripes, "hor. str." denotes horizontal stripes, "con. cir." denotes concentric circles, "lin. grad." linear gradient, "rad. grad." denotes radial gradient, "con. rgs." denotes concentric rings, "cr. hatch" denotes cross hatch categories.

Feat.	Pattern	Qwen7b	Qwen32b	Intern	Kim
Bg	Color blue	0.154	0.142	0.103	0.079
Bg	Color black	0.170	0.143	0.115	0.080
Bg	Color green	0.235	0.112	0.112	0.145
Bg	Color gray	0.254	0.135	0.138	0.078
Bg	Color red	0.311	0.129	0.131	0.247
Bg	Color yellow	0.318	0.138	0.198	0.341
Bg	Texture noise	0.234	0.121	0.128	0.086
Bg	Texture cr. hatch	0.355	0.141	0.122	0.078
Bg	Texture lin. grad.	0.504	0.115	0.078	0.084
Bg	Texture rad. grad.	0.572	0.120	0.100	0.139
Bg	Texture checkerboa	0.832	0.141	0.160	0.432
Bg	Texture dots	0.803	0.184	0.144	0.453
Bg	Texture diag. str.	0.751	0.163	0.098	0.687
Bg	Texture con. rgs	0.723	0.270	0.198	0.627
Bg	Texture hor. str.	0.734	0.306	0.109	0.757
Bg	Texture ver. str.	0.695	0.413	0.153	0.773
Bg	Texture bubbles	0.888	1.209	1.203	0.845
Obj	Color white	0.210	0.066	0.102	0.098
Obj	Color red	0.187	0.130	0.084	0.084
Obj	Color yellow	0.201	0.113	0.082	0.116
Obj	Color blue	0.217	0.130	0.108	0.068
Obj	Color light gray	0.215	0.088	0.158	0.097
Obj	Color green	0.335	0.075	0.081	0.078
Obj	Color multicolor	0.553	0.129	0.081	0.350
Obj	Shape star	0.216	0.143	0.083	0.077
Obj	Shape circle	0.178	0.137	0.154	0.072
Obj	Shape rectangle	0.390	0.123	0.195	0.085
Obj	Shape polygon	0.397	0.118	0.140	0.138
Obj	Shape triangle	0.493	0.154	0.069	0.320
Obj	Texture rad. grad.	0.200	0.124	0.085	0.074
Obj	Texture dots	0.462	0.143	0.132	0.071
Obj	Texture con. cir.	0.576	0.075	0.106	0.073
Obj	Texture lin. grad.	0.576	0.113	0.077	0.067
Obj	Texture cr. hatch	0.617	0.076	0.101	0.079
Obj	Texture checkerboa	0.644	0.110	0.101	0.062
Obj	Texture ver. str.	0.617	0.128	0.089	0.092
Obj	Texture zigzag	0.551	0.148	0.153	0.079
Obj	Texture diag. str.	0.548	0.198	0.125	0.068
Obj	Texture hor. str.	0.605	0.342	0.156	0.089

Table 13. Mean Relative Count Error (lower is better) for Prompt 3 across all patterns. “Bg” denotes *Background*, “Obj” denotes *Object* and ”diag. str.” denotes diagonal stripes, ”ver. str.” denotes vertical stripes, ”hor. str.” denotes horizontal stripes, ”con. cir.” denotes concentric circles, ”lin. grad.” linear gradient, ”rad. grad.” denotes radial gradient, ”con. rgs.” denotes concentric rings, ”cr. hatch” denotes cross hatch categories.

Cat.	Feat.	Pattern	Qwen7b	Qwen32b	Intern	Kimi
Bg	Color	blue	0.142	0.096	0.130	0.064
Bg	Color	green	0.164	0.092	0.143	0.070
Bg	Color	black	0.168	0.085	0.141	0.079
Bg	Color	red	0.166	0.099	0.176	0.067
Bg	Color	gray	0.186	0.106	0.159	0.076
Bg	Color	yellow	0.190	0.096	0.216	0.094
Bg	Texture	lin. grad.	0.164	0.093	0.072	0.098
Bg	Texture	noise	0.144	0.092	0.161	0.073
Bg	Texture	rad. grad.	0.179	0.138	0.137	0.078
Bg	Texture	ver. str.	0.224	0.183	0.203	0.077
Bg	Texture	checkerboa	0.243	0.166	0.187	0.121
Bg	Texture	dots	0.280	0.183	0.173	0.107
Bg	Texture	hor. str.	0.246	0.219	0.126	0.167
Bg	Texture	con. rgs	0.254	0.186	0.261	0.070
Bg	Texture	cr. hatch	0.201	0.495	0.140	0.067
Bg	Texture	diag. str.	0.260	0.411	0.162	0.082
Bg	Texture	bubbles	0.271	0.196	0.344	0.205
Obj	Color	green	0.102	0.064	0.074	0.077
Obj	Color	blue	0.105	0.092	0.106	0.062
Obj	Color	red	0.126	0.108	0.088	0.067
Obj	Color	yellow	0.142	0.058	0.093	0.108
Obj	Color	white	0.111	0.125	0.128	0.130
Obj	Color	light gray	0.176	0.113	0.188	0.085
Obj	Color	multicolor	0.319	0.279	0.259	0.313
Obj	Shape	polygon	0.112	0.084	0.148	0.082
Obj	Shape	star	0.148	0.144	0.090	0.085
Obj	Shape	circle	0.182	0.134	0.182	0.076
Obj	Shape	triangle	0.101	0.148	0.088	0.281
Obj	Shape	rectangle	0.169	0.176	0.230	0.082
Obj	Texture	con. cir.	0.124	0.104	0.170	0.070
Obj	Texture	ver. str.	0.179	0.183	0.164	0.084
Obj	Texture	hor. str.	0.194	0.219	0.188	0.083
Obj	Texture	lin. grad.	0.176	0.093	0.421	0.077
Obj	Texture	dots	0.270	0.183	0.310	0.065
Obj	Texture	rad. grad.	0.217	0.138	0.432	0.085
Obj	Texture	checkerboa	0.355	0.326	0.492	0.078
Obj	Texture	zigzag	0.261	0.369	0.677	0.088
Obj	Texture	diag. str.	0.504	0.411	0.535	0.091
Obj	Texture	cr. hatch	0.490	0.495	0.819	0.301

Table 14. Mean Relative Count Error (lower is better) for Prompt 4 across all patterns. “Bg” denotes *Background*, “Obj” denotes *Object* and ”diag. str.” denotes diagonal stripes, ”ver. str.” denotes vertical stripes, ”hor. str.” denotes horizontal stripes, ”con. cir.” denotes concentric circles, ”lin. grad.” linear gradient, ”rad. grad.” denotes radial gradient, ”con. rgs.” denotes concentric rings, ”cr. hatch” denotes cross hatch categories.

Cat.	Feat.	Pattern	Qwen7b	Qwen32b	Intern	Kimi
Bg	Texture	lin. grad.	0.183	0.103	0.112	0.079
Bg	Texture	noise	0.137	0.089	0.197	0.070
Bg	Texture	rad. grad.	0.187	0.138	0.135	0.063
Bg	Texture	cr. hatch	0.192	0.138	0.172	0.105
Bg	Texture	checkerboa	0.245	0.122	0.194	0.083
Bg	Texture	hor. str.	0.272	0.133	0.144	0.108
Bg	Texture	ver. str.	0.232	0.139	0.216	0.087
Bg	Texture	dots	0.271	0.143	0.200	0.106
Bg	Texture	diag. str.	0.273	0.154	0.191	0.131
Bg	Texture	con. rgs	0.287	0.158	0.268	0.091
Bg	Texture	bubbles	0.261	0.163	0.346	0.230
Obj	Texture	con. cir.	0.185	0.104	0.177	0.075
Obj	Texture	rad. grad.	0.194	0.129	0.218	0.117
Obj	Texture	lin. grad.	0.190	0.108	0.268	0.101
Obj	Texture	ver. str.	0.187	0.181	0.258	0.072
Obj	Texture	hor. str.	0.243	0.199	0.266	0.094
Obj	Texture	dots	0.219	0.298	0.166	0.166
Obj	Texture	zigzag	0.239	0.228	0.341	0.098
Obj	Texture	checkerboa	0.387	0.311	0.433	0.087
Obj	Texture	diag. str.	0.516	0.457	0.594	0.056
Obj	Texture	cr. hatch	0.679	0.873	0.419	0.798

Table 15. Mean Relative Count Error (lower is better) for Prompt 5 across all patterns. “Bg” denotes *Background*, “Obj” denotes *Object* and ”diag. str.” denotes diagonal stripes, ”ver. str.” denotes vertical stripes, ”hor. str.” denotes horizontal stripes, ”con. cir.” denotes concentric circles, ”lin. grad.” linear gradient, ”rad. grad.” denotes radial gradient, ”con. rgs.” denotes concentric rings, ”cr. hatch” denotes cross hatch categories.

Cat.	Feat.	Pattern	Qwen7b	Qwen32b	Intern	Kimi
Bg	Texture	noise	0.152	0.069	0.203	0.067
Bg	Texture	lin. grad.	0.185	0.109	0.126	0.081
Bg	Texture	rad. grad.	0.192	0.121	0.153	0.065
Bg	Texture	cr. hatch	0.211	0.111	0.175	0.071
Bg	Texture	hor. str.	0.270	0.114	0.143	0.120
Bg	Texture	checkerboa	0.252	0.123	0.188	0.098
Bg	Texture	ver. str.	0.234	0.146	0.222	0.087
Bg	Texture	dots	0.293	0.106	0.211	0.114
Bg	Texture	diag. str.	0.282	0.163	0.202	0.110
Bg	Texture	con. rgs	0.295	0.189	0.283	0.103
Bg	Texture	bubbles	0.269	0.187	0.360	0.191
Obj	Texture	con. cir.	0.198	0.082	0.190	0.081
Obj	Texture	lin. grad.	0.175	0.114	0.241	0.103
Obj	Texture	rad. grad.	0.206	0.126	0.199	0.117
Obj	Texture	ver. str.	0.219	0.205	0.245	0.083
Obj	Texture	hor. str.	0.284	0.205	0.269	0.087
Obj	Texture	zigzag	0.240	0.307	0.318	0.110
Obj	Texture	dots	0.245	0.416	0.186	0.187
Obj	Texture	checkerboa	0.397	0.338	0.414	0.094
Obj	Texture	diag. str.	0.532	0.482	0.603	0.088
Obj	Texture	cr. hatch	0.745	0.893	0.404	0.786